ISSN (Print) 1226-1750
ISSN (Online) 2233-6656
Journal of Magnetics 26(4), 394-400 (2021) https://doi.org/10.4283/JMAG.2021.26.4.394

Enhanced Hard-magnetic Properties of Rare Earth-free $L1_0$-FeNi Phase in FeNiPC Alloys

Jonghee Han[1†], Jin-Yoo Suh[2†], Hyunsol Son[1], and Haein Choi-Yim[1*]

[1]*Department of Applied Physics, Sookmyung Women's University, Seoul 04310, South Korea*
[2]*Center for Energy Materials Research, Korea Institute of Science and Technology, Seoul 02792, South Korea*

(Received 1 December 2021, Received in final form 22 December 2021, Accepted 23 December 2021)

In this study, FeNi-based amorphous alloys having crystallization temperature (T_x) close to FeNi order-disorder transition temperature were developed. Through an extended annealing process at around the crystallization temperature, an ordered phase, $L1_0$-FeNi, was formed. Structural characterizations of annealed ribbons confirmed the formation of $L1_0$-FeNi phase through observation of a weak superlattice peak. Measured coercivity (H_c) also indicated formation of the ordered $L1_0$-FeNi phase, which increased up to 744 Oe after the annealing process.

Keywords : $L1_0$-FeNi phase, hard-magnetic properties, melt spun ribbon

1. Introduction

Demand for permanent magnets has rapidly increased with growing demands on electrical applications such as motors, automobiles, and renewable-energy devices [1-5]. Rare earth compounds are well known as suitable materials for permanent magnets owing to their superior magnetic properties, such as high saturation magnetization (M_s) and high maximum magnetic energy product (BH_{max}). However, rare earth materials as indicated by their name are not abundant on earth resulting in an unbalanced supply-demand relationship [6]. In addition, severe environmental pollution has occurred by the excessive use of rare earth resources [7]. Therefore, development of novel rare-earth-free permanent magnets is crucial to reduce the dependence on rare-earth resources. Rare-earth-free permanent magnetic materials such as ferrite, LTP (Low temperature phase)-MnBi, $L1_0$-FePt, α′-FeN, and $L1_0$-FeNi have been extensively studied [8-12]. Among these materials, $L1_0$-FeNi phase appears one of the strongest candidates. $L1_0$-FeNi phase exhibits superior magnetic properties, exhibiting a large M_s (~1270 emu/cm^3), large uniaxial magnetic anisotropy (K_u of ~1.3×10^7 erg/cm^3), and high theoretical BH_{max} (~42 MG Oe) [13, 14]. Furthermore, Curie temperature (T_c) of $L1_0$-FeNi is higher (~550 °C) than that of NdFeB-based magnets [15]. In addition, $L1_0$-FeNi phase is cost-effective because it consists of Fe and Ni, which are both abundant and inexpensive compared to other non-rare earth elements [16].

$L1_0$-FeNi phase was first discovered in a meteorite named NWA 6259 [17]. In this meteorite, the ordered $L1_0$-FeNi phase appeared together with a disordered (Face-centered Cubic, FCC) FeNi phase as a result of phase transition from the fcc phase to the ordered ($L1_0$) phase through an extremely slow cooling rate of approximately 1 °C/10^6 years of the universe [18]. The order-disorder transition temperature at which the phase transition from FCC- to $L1_0$-phase appears is relatively low (~320 °C) [19], at which the diffusion coefficients of Fe and Ni are also very low [18]. Therefore, it is difficult to artificially form the $L1_0$-FeNi phase for a bulk-shaped magnet based on the previously reported methods, such as high-energy ball milling, thin film growth, irradiation with high-energy beams, or high-energy torsion techniques [18, 20-23]. As an alternative way to acquire the product of transformation of extremely slow kinetics, researchers fabricated an amorphous ribbon of an FeNi-based alloy by melt-spinning and carried out heat treatment carefully to induce crystallization from amorphous state at around the order-disorder transition temperature [18, 24-27]. Motivated by those pioneering works, to further develop

†These authors contributed equally to this work.

*Corresponding author: Tel: +82-2-710-9239
e-mail: haein@sookmyung.ac.kr

the idea in this study, FeNi-based alloys with a crystallization temperature (T_x) of approximately the same value as that of the order-disorder transition temperature were developed. Herein, the enhancement of hard-magnetic properties, such as coercivity (H_c), was addressed, and the obtained value was compared with previously reported data (~700 Oe) [27].

2. Experimental

Fe-Ni-based ingots with nominal compositions of $[Fe_{0.5}Ni_{0.5}]_x[P_{0.65}C_{0.25}]_{100-x}$ (x = 81, 82, and 83 at.%) were prepared by induction melting of mixtures containing high-purity elemental materials, which were re-melted using an arc melter in a Ti-gettered Ar atmosphere to ensure homogeneity. Amorphous ribbons were produced by melt-spinning under Ar atmosphere with a wheel speed of 56.3 m/s. The width and thickness of the ribbons were 2 mm and 20-30 μm, respectively. Prior to the annealing treatment to produce the crystalline phase, the as-spun ribbons were sealed in a quartz tube containing Ar and annealed in a box furnace that was preheated to annealing temperature. The annealing temperature was set to be around T_x of the as-spun amorphous ribbons. The values of T_x were measured by differential scanning calorimetry (DSC) at a heating rate of 0.34 °C/s. The structural properties of both the as-spun and annealed ribbons were observed by X-ray diffraction (XRD). The microstructures of the annealed ribbons were examined by transmission electron microscopy (TEM). Further, magnetic properties of the alloys, such as M_s and H_c, were measured using a vibrating sample magnetometer (VSM) at room temperature. These magnetic properties were recorded in a maximum applied field of 10 kOe at different incident angles (θ).

3. Results and Discussion

To optimize the annealing conditions, thermal properties of the as-spun $[Fe_{0.5}Ni_{0.5}]_x[P_{0.65}C_{0.25}]_{100-x}$ (x = 81, 82, and 83 at.%) alloys were investigated to determine the annealing temperature (T_a). Figure 1 shows the DSC curves of the alloys. The difference between the first crystallization temperature (T_{x1}) and the second crystallization temperature (T_{x2}) increased with increasing FeNi content, as shown in Fig. 1. In addition, as the Fe content increased, T_{x1} decreased to approach closer to the order-disorder transition temperature of $L1_0$-FeNi (~320 °C). When the temperature interval between different crystallization peaks increases, the first crystallization (which is expected to be the formation of FCC FeNi solid solution phase) dominates the early stage crystallization and, therefore, the formation of the $L1_0$-FeNi phase could possibly be favored. It has been reported that the crystallization temperature intervals might increase as the Fe content increases [28]. Annealing treatments on the amorphous ribbons were carried out at different temperatures close to T_{x1} of each alloy for 288 h as shown in Table 1.

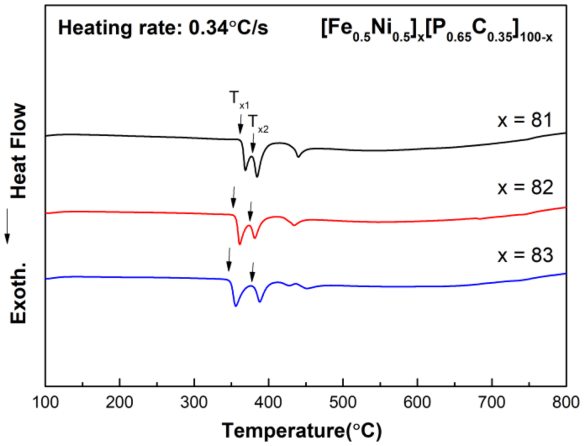

Fig. 1. (Color online) DSC curves of the as-spun $[Fe_{0.5}Ni_{0.5}]_x[P_{0.65}C_{0.25}]_{100-x}$ (x = 81, 82, and 83 at.%) ribbons.

Makino *et al*. also reported that the annealing around the first crystallization onset temperature worked successfully for the synthesis of $L1_0$-FeNi, which was indirectly proven by that the annealed alloys exhibited high hard-magnetic properties [18]. The values of T_x and T_a are summarized in Table 1. Figures 2(a) and (b) show the XRD patterns of the as-spun samples. In Fig. 2(a), broad humps without the presence of crystalline peaks are observed for all three ribbons indicating that the struc-

Table 1. Crystallization and annealing temperatures at different compositions of the $[Fe_{0.5}Ni_{0.5}]_x[P_{0.65}C_{0.25}]_{100-x}$ alloy (x = 81, 82, and 83).

Composition (at. %) $[Fe_{0.5}Ni_{0.5}]_x[P_{0.65}C_{0.25}]_{100-x}$	T_{x1} (°C)	$\Delta(T_{x1}$-$T_{x2})$	T_{x2}	T_{x3}	T_{x4}	T_a
x = 81	362	15	377	431	-	360
x = 82	356	18	474	416	-	355
x = 83	347	32	479	413	435	350

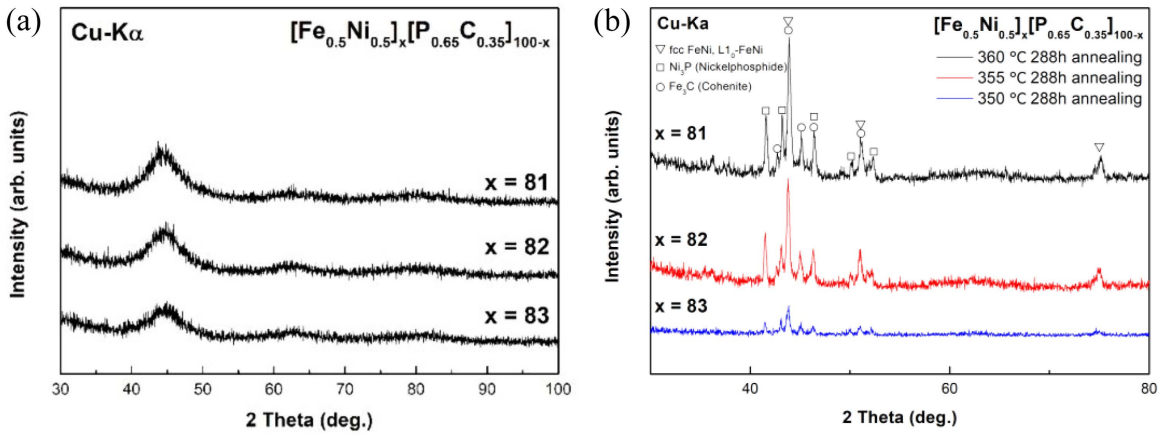

Fig. 2. (Color online) XRD patterns of (a) the as-spun and (b) annealed $[Fe_{0.5}Ni_{0.5}]_x[P_{0.65}C_{0.25}]_{100-x}$ (x = 81, 82, and 83 at.%) ribbons.

tures of the samples are dominantly amorphous. As shown in Fig. 2(b), crystalline peaks were observed for the annealed ribbons, including the disordered (FCC) FeNi, the ordered $L1_0$-FeNi, nickel phosphide ($FeNi_2P$), and cohenite (Fe_3C). XRD was conducted to observe the formation of the $L1_0$-FeNi phase by detecting superlattice peaks of the ordered phase because the XRD pattern of the $L1_0$-FeNi phase was similar to that of the disordered (FCC) phase of FeNi with only difference in the superlattice peaks [12, 29].

However, those superlattice peaks were not evident in the XRD data because of the limited intensity of the superlattice peaks compared to other regular peaks. Therefore, characterization using a synchrotron X-ray diffractometer equipped with high beam flux was carried out (Fig. 3) to observe the superlattice peaks of annealed $[Fe_{0.5}Ni_{0.5}]_{81}[P_{0.65}C_{0.25}]_{19}$ ribbon. As shown in the synchrotron XRD pattern of $[Fe_{0.5}Ni_{0.5}]_{81}[P_{0.65}C_{0.25}]_{19}$ with wavelength of 0.152250 nm which is close to that of Cu Kα radiation (0.154059 nm), the (100) superlattice peak appeared at ~35.2°, which is a right shoulder of a peak at ~35° (Figs. 3(a) and (b)) (Please note that (100) indicates the plane of a tetragonal system, P4/mmm, a=0.2533 nm and c=0.3607 [16]).

Figure 4 shows the magnetic hysteresis loops of the as-spun $[Fe_{0.5}Ni_{0.5}]_x[P_{0.65}C_{0.25}]_{100-x}$ (x = 81, 82, and 83 at.%)

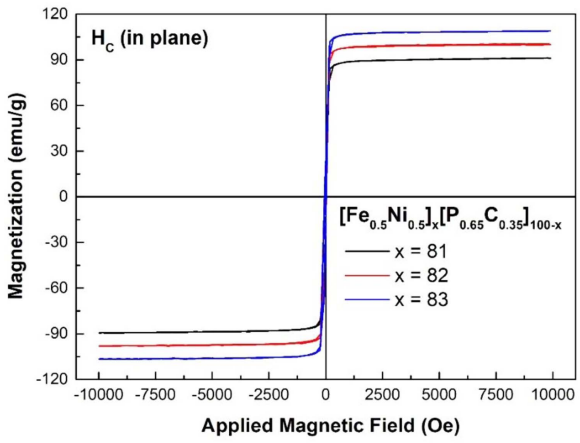

Fig. 4. (Color online) Hysteresis loops of the as-spun $[Fe_{0.5}Ni_{0.5}]_x[P_{0.65}C_{0.25}]_{100-x}$ (x = 81, 82, and 83 at.%) ribbons.

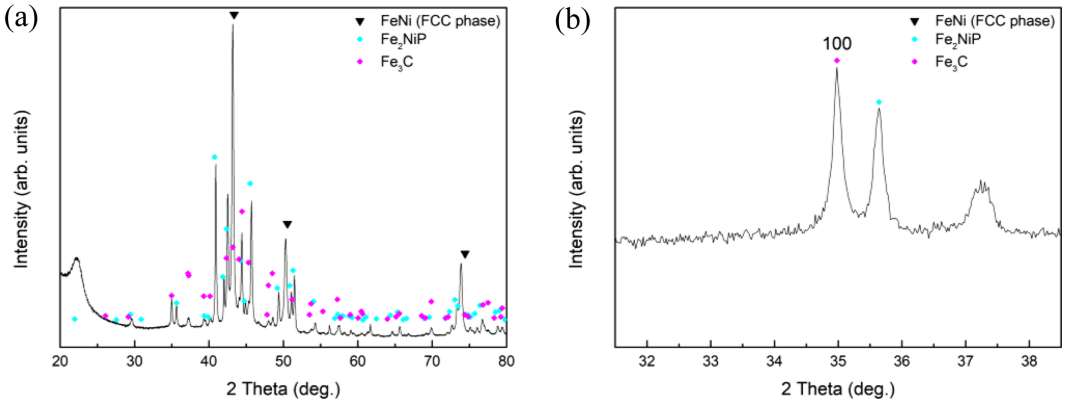

Fig. 3. (Color online) (a) Synchrotron XRD patterns of the annealed $[Fe_{0.5}Ni_{0.5}]_{81}[P_{0.65}C_{0.25}]_{19}$ ribbon and magnified view at surrounding regions near 2θ of (b) 35°.

Table 2. H_c values of the annealed $[Fe_{0.5}Ni_{0.5}]_x[P_{0.65}C_{0.25}]_{100-x}$ (x = 81, 82, and 83 at.%) ribbons.

Degree (°)	$[Fe_{0.5}Ni_{0.5}]_x[P_{0.65}C_{0.25}]_{100-x}$		
	$x = 81$	$x = 82$	$x = 83$
	H_c (Oe)		
0 (in-plane)	299	306	238
10	309	326	245
20	326	330	262
30	351	347	300
40	386	380	338
50	449	441	386
60	553	547	502
70	581	698	586
80	744	700	664
90 (out-of-plane)	491	472	503

ribbons measured by VSM. The M_s values of the as-spun ribbons ranged from 90 to 108 emu/g with increasing FeNi ratio. The H_c values were low, ranging from 37 to 34.5 Oe, which confirmed the presence of typical soft-magnetic materials. However, after the annealing process, both the in-plane and out-of-plane data showed significantly increased H_c. As listed in Table 2, the highest H_c values of $[Fe_{0.5}Ni_{0.5}]_x[P_{0.65}C_{0.25}]_{100-x}$ (x = 81, 82, and 83 at.%) alloys annealed at T_a, 360, 355, and 350 °C for 288 h were 744, 700, and 664 Oe, respectively. The highest H_c for all alloy samples were observed at 80° (Table 2). These results were similar to previously reported data from a meteorite analysis, which exhibited an optimum magnetization curve at 82° [30]. The H_c enhancement (Fig. 5) was possibly because of the formation of the $L1_0$-FeNi phase (i.e., the hard-magnetic phase) after annealing, which was further confirmed by the structural analysis. When a magnetic field was applied at about 80° with respect to the ribbon plane, the large magnetization increase at lower magnetic field was possibly owing to the c-axis magnetic anisotropy of the $L1_0$-FeNi phase. In addition, α-Fe and Fe_3B phases, although those phases were not observed in this study, which have magnetic easy axes at the ribbon plane could contribute to linear increase in magnetization at higher fields [18]. Such a linear increase in magnetization was also observed for the meteorites.

The phases other than $L1_0$-FeNi, such as the nickel phosphide ($FeNi_2P$) and cohenite (Fe_3C) phases, are not hard-magnetic. Also, it should be noted that iron with BCC structure, which is a strong hard-magnet, was not formed by annealing in this study. Studies regarding the phases that can affect H_c in FCC Fe have been reported previously. Jiles *et al*. obtained a maximum H_c value of

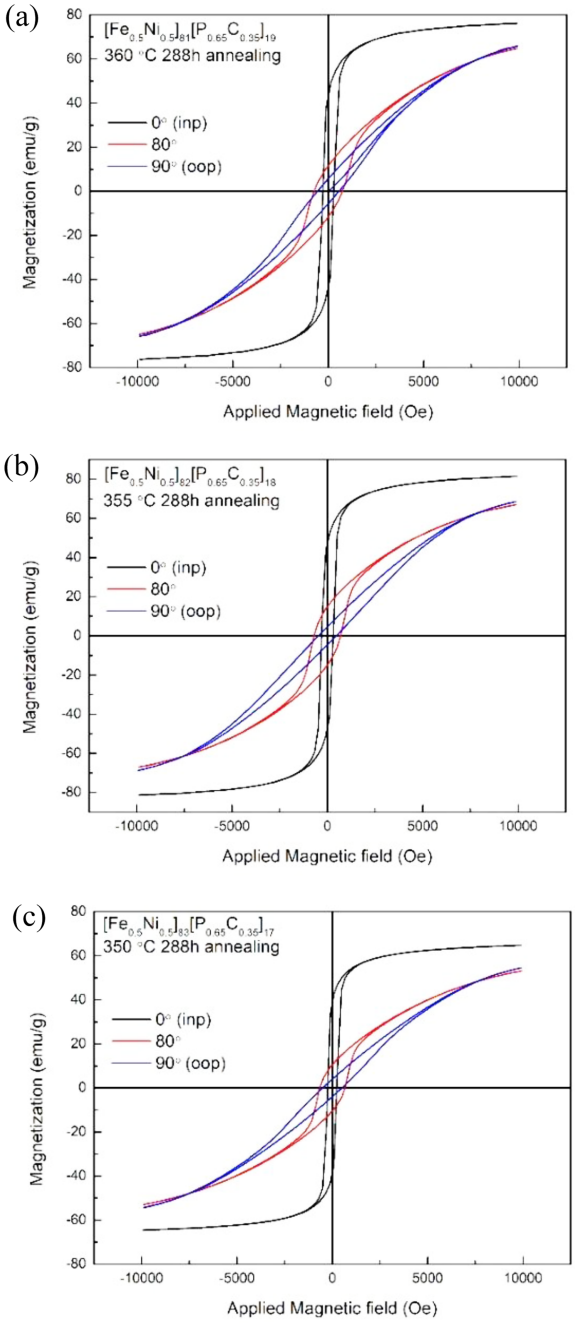

Fig. 5. (Color online) Hysteresis loops of the annealed (a) $[Fe_{0.5}Ni_{0.5}]_{81}[P_{0.65}C_{0.25}]_{19}$, (b) $[Fe_{0.5}Ni_{0.5}]_{82}[P_{0.65}C_{0.25}]_{18}$, and (c) $[Fe_{0.5}Ni_{0.5}]_{83}[P_{0.65}C_{0.25}]_{17}$ ribbons.

~2 Oe (FCC Fe phase) when the phase diameter was in the range of 8-11 μm [31]. Carbide inclusions in carbon steels can also increase the H_c value, leading to a maximum value of ~10 Oe [32]. However, these H_c values are significantly low compared to those of the annealed $[Fe_{0.5}Ni_{0.5}]_x[P_{0.65}C_{0.25}]_{100-x}$ (x = 81, 82, and 83 at.%) ribbons (H_c in the range of 664-744 Oe). The higher H_c values are most likely to indicate the formation of the $L1_0$-FeNi

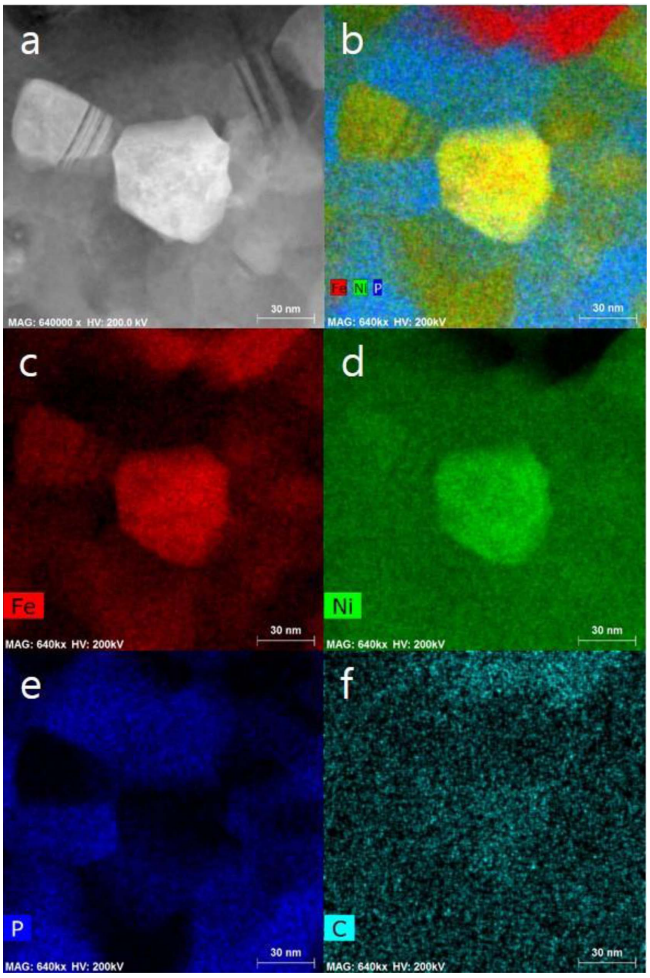

Fig. 6. (Color online) (a) STEM-HAADF image and (b–f) EDS elemental maps of the annealed $[Fe_{0.5}Ni_{0.5}]_{81}[P_{0.65}C_{0.25}]_{19}$ ribbon prepared at 360 °C (T_{x1}) for 288 h.

phase. Thus, it was concluded that the $L1_0$-FeNi phase precipitated in the annealed $[Fe_{0.5}Ni_{0.5}]_x[P_{0.65}C_{0.25}]_{100-x}$ (x = 81, 82, and 83 at.%) ribbons, which was reflected by the highest H_c value at 80°.

For microstructural investigation of the $L1_0$-FeNi phase, TEM and EDS were performed. Figure 6 shows the STEM-HAADF (Scanning Transmission Electron Microscopy – High Angle Annular Dark Field) image and EDS maps of the major elements of the $[Fe_{0.5}Ni_{0.5}]_{81}[P_{0.65}C_{0.25}]_{19}$ ribbon annealed at 360 °C for 288 h. EDS mapping provided the distribution of Fe, Ni, and P; however, the distribution of C was not clearly observed. In the integrated EDS map (Fig. 6(b)), the nearly equiatomic FeNi phase was observed in the center part of the figure. The quantified compositions of the Fe- and Ni-rich regions were consistent with the indexing results of XRD for cohenite (Fe_3C, Fig. 6(c) and (f)) and nickel phosphide ($FeNi_2P$, Fig. 6(d) and (f)), respectively, as shown in Figs.

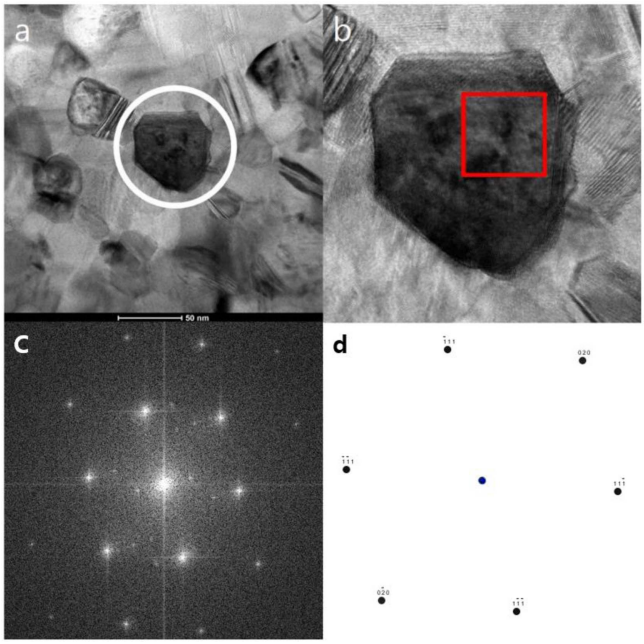

Fig. 7. (Color online) (a), (b) Bright field TEM images; (c) SAED pattern; (d) FFT diffraction patterns of the annealed ribbons at 360 °C (T_{x1}) for 576 h.

2 and 3. The chemical composition of the FeNi equiatomic phase was calculated to be ~39, ~58, and ~3 at% for Fe, Ni, and P, respectively, which is comparable to the ideal Fe:Ni ratio of the phase [28]. Similar results for the phase distribution and chemical compositions of the constituent phases were also acquired for the ribbon specimens of x=82 and 83 annealed at 355 and 350 °C, respectively, for 288 h. Figures 7(a) and (b) (marked regions) correspond to the FeNi equiatomic phase based on the composition data (same location as the one shown in Fig. 6). Figure 7(b) is a high-resolution image of Fig. 7(a) providing diffraction pattern created by fast Fourier transform (FFT) of Fig. 7(b) (Fig. 7(c)). In Fig. 7(c), the fcc-lattice spots can be clearly observed with (111) and (020) reflections along the (110)-zone axis as confirmed by calculated diffraction pattern shown in Fig. 7(d). However, the superlattice reflections were quite weak and not visible in this observation (Fig. 7(c)). The reason for not being able to detect the ordering of the FeNi phase from TEM observation could be that the ordering could have taken place only partially in every FeNi precipitates that the diffraction from the ordered part is too weak to be detected from the conventional TEM work. The grain size of the annealed ribbons was rather small (~60 nm) and a wide defect zone (Moire fringes) appeared because of the grain overlapping along the thickness direction of the TEM specimen. Although the $L1_0$ phase formation was not detected by TEM, the synchrotron XRD patterns (Fig.

3) and the values of H_c (Fig. 5) comprised experimental evidence of the precipitation of the $L1_0$ phase.

4. Conclusion

Herein, $[Fe_{0.5}Ni_{0.5}]_x[P_{0.65}C_{0.25}]_{100-x}$ (x = 81, 82, and 83 at.%) amorphous alloys with enhanced hard-magnetic properties were fabricated through crystallization heat treatment which is believed to have induced the formation of the $L1_0$-FeNi phase in the ribbons. To artificially produce the hard-magnetic $L1_0$-FeNi phase, the amorphous ribbons produced by melt-spinning were annealed at different T_a values that almost corresponded to the T_x of each alloy. And, T_x of the alloys was not much different from the known order-disorder transition temperature of FeNi alloy. The results of this study are summarized as follows:

(1) As-spun $[Fe_{0.5}Ni_{0.5}]_x[P_{0.65}C_{0.25}]_{100-x}$ (x = 81, 82, and 83 at.%) ribbons exhibited a typical amorphous structure. However, the ribbons annealed at different T_a for 288 h were comprised of crystalline peaks of different phases including disordered FCC FeNi, Fe_3C, $FeNi_2P$, and ordered $L1_0$-FeNi. To confirm the superlattice peaks of the ordered $L1_0$-FeNi phase, structural analyses were conducted using synchrotron XRD. The (100)-superlattice peaks were observed through the high beam flux of the irradiating synchrotron X-ray. Thus, the precipitation of the ordered $L1_0$-FeNi phase was confirmed.

(2) Among the annealed $[Fe_{0.5}Ni_{0.5}]_x[P_{0.65}C_{0.25}]_{100-x}$ (x = 81, 82, and 83 at.%) ribbons, the ribbons containing the $L1_0$-FeNi phase with c-axis magnetic anisotropy had lower H_c values along the in-plane direction of the ribbon. However, they exhibited the highest H_c values at 80° with respect to the ribbon plane. The H_c enhancement also supports the formation of a hard-magnetic phase ($L1_0$-FeNi phase) after annealing.

(3) For microstructural analysis, the annealed ribbons were examined by TEM observation together with EDS mapping. Fe-rich, Ni-rich, and almost FeNi equiatomic regions were observed in the annealed $[Fe_{0.5}Ni_{0.5}]_x$-$[P_{0.65}C_{0.25}]_{100-x}$ (x = 81, 82, and 83 at.%) ribbons. High resolution imaging and FFT for detecting the $L1_0$-FeNi phase in the FeNi equiatomic regions turned out not to work which might suggest that ordering of FeNi precipitates took place only partially.

Acknowledgments

This work has supported by the National Research Foundation of Korea (NRF) grant funded by the Korea government (MSIT) (No.2021R1A2C2008220).

References

[1] R. Skomski and J. M. D. Coey, Permanent magnetism, Institute of Physics, Bristol (1999).
[2] S. Chikazumi, Physics of Magnetism, Wiley, New York (1964).
[3] R. Skomski and J. M. D. Coey, Scr. Mater. **112**, 3 (2016).
[4] O. Gutfleisch, M. A. Willard, E. Brück, C. H. Chen, S. G. Sankar, and J. P. Liu, Adv. Mater. **23**, 821 (2011).
[5] J. M. D. Coey, J. Magn. Magn. Mater. **248**, 441 (2002).
[6] T. Dutta, K. H. Kim, M. Uchimiya, E. E. Kwon, B. H. Jeon, A. Deep, and S. T. Yun, Environ. Res. **150**, 182 (2016).
[7] S. Massari, M. Ruberti, Resour. Policy **38**, 36 (2013).
[8] N. Rezlescu, E. Rezlescu, C. Pasnicu, and M. L. Craus, J. Phys.: Condens. Matter **6**, 5707 (1994).
[9] J. B. Yang, K. Kamaraju, W. B. Yelon, W. J. James, Q. Cai, and A. Bollero, Appl. Phys. Lett. **79**, 1846 (2001).
[10] B. Zhang and W. A. Soffa, Scr. Metall. Mater. **30**, 683 (1994).
[11] J. M. D. Coey, K. O'Donnell, Q. Qinian, E. Touchais, and K. H. Jack, J. Phys.: Condens. Matter **6**, L23 (1994).
[12] R. S. Clarke Jr. and E. R. D. Scott, Am. Mineral. **65**, 624 (1980).
[13] L. H. Lewis, F. E. Pinkerton, N. Bordeaux, A. Mubarok, E. Poirier, J. I. Goldstein, R. Skomski, and K. Barmak, IEEE Magn. Lett. **5**, 5500104 (2014).
[14] J. Paulevé, A. Chamberod, K. Krebs, and A. Bourret, J. Appl. Phys. **39**, 989 (1968).
[15] T. Kojima *et al.*, J. Phys.: Condens. Matter **26**, 064207 (2014).
[16] M. Kotsugi, H. Maruyama, N. Ishimatsu, N. Kawamura, M. Suzuki, M. Mizumaki, K. Osaka, T. Matsumoto, T. Ohkochi, T. Ohtsuki, T. Kojima, M. Mizuguchi, K. Takanashi, and Y. Watanabe, J. Phys.: Condens. Matter **26**, 064206 (2014).
[17] L. Néel, J. Pauleve, R. Pauthenet, J. Laugier, and D. Dautreppe, J. Appl. Phys. **35**, 873 (1964).
[18] A. Makino, P. Sharma, K. Sato, A. Takeuchi, Y. Zhang, and K. Takenaka, Sci. Rep. **5**, 16627 (2015).
[19] J. F. Albertsen, J. M. Knudsen, N. O. Roy-Poulsen, and L. Vistisen, Phys. Scr. **22**, 171 (1980).
[20] M. Kotsugi, M. Mizuguchi, S. Sekiya, T. Ohkouchi, T. Kojima, K. Takanashi, and Y. Watanabe, J. Phys.: Conf. Ser. **266**, 012095 (2011).
[21] T. Kojima, M. Mizuguchi, and K. Takanashi, Thin Solid Films **603**, 348 (2016).
[22] S. Lee, K. Edalati, H. Iwaoka, Z. Horita, T. Ohtsuki, and T. Ohkochi, Philos. Mag. Lett. **94**, 639 (2014).
[23] K. Sato, P. Sharma, Y. Zhang, K. Takenaka, and A. Makino, AIP Adv. **6**, 055218 (2016).
[24] Q. Li, J. Li, P. Gong, K. Yao, J. Gao, and H. Li, Intermetallics **26**, 62 (2012).
[25] W. Zhang, C. Fang, and Y. Li, Scr. Mater. **69**, 77 (2013).
[26] A. Inoue, T. Zhang, H. Koshiba, and A. Makino, J. Appl.

Phys. **83**, 6326 (1998).
[27] J. Kim, S. Kim, J. Y. Suh, Y. J. Kim, Y. K. Kim, and H. Choi-Yim, Curr. Appl. Phys. **19**, 599 (2019).
[28] K. Xu, H. Ling, Q. Li, J. Li, K. Yao, and S. Guo, Intermetallics **51**, 53 (2014).
[29] V. D. Dobrovol skii, S. M. Karal nuk, and A. V. Koval, Metallofizika **41**, 73 (1972).
[30] E. Poirier, F. E. Pinkerton, R. Kubic, R. K. Mishra, N. Bordeaux, A. Mubarok, L. H. Lewis, J. I. Goldstein, R. Skomski, and K. Barmak, J. Appl. Phys. **117**, 17e318 (2015).
[31] D. C. Jiles, C. V. Owen, and W. A. Spitzig, J. Nondestr. Eval. **6**, 119 (1987).
[32] D. C. Jiles, J. Phys. D **21**, 1186 (1987).